

Automatic levee surface extraction from mobile LiDAR data using directional equalization and projection clustering

Jisang Lee, Suhong Yoo, Cheolhwan Kim, Hong-Gyoo Sohn*

Department of Civil and Environmental Engineering, Yonsei University, 50 Yonsei-ro, Seodaemun-gu, Seoul 03722, South Korea



ARTICLE INFO

Keywords:
Mobile laser scanner
Point cloud filtering
Levee management
Digital twin

ABSTRACT

A levee is an engineering structure that physically suppresses flooding by directly touching the river. Enough levee elevation prevents water from overflowing the levee. Therefore, obtaining the physical shape of the river levee is the starting point of levee management based on the digital twin. Total station, global navigation satellite system (GNSS), or small unmanned aircraft systems (sUASs) have been used to investigate the physical shape of the levee. However, there are economical and temporal limitations in applying these methods to the entire levee alignment installed in more than ten thousand kilometers along the water system. Mobile laser scanner (MLS) mounted on a vehicle can resolve the problem because it moves at high speeds for a long time. Therefore, many researchers are conducting studies acquiring geospatial data with vehicle-type MLS. MLS collects data in point cloud form with locational information. Ground filtering algorithms for point clouds have been studied in order to obtain the physical shape of the levee from point clouds. However, since existing ground filtering algorithms are mostly designed for airborne laser scanner (ALS)- or terrestrial laser scanner (TLS)-based data, they have limitations in applying to point cloud data acquired from MLS. Therefore, we developed an algorithm to extract levee point cloud from MLS-acquired point cloud data. The algorithm contains several methodologies named directional equalization and point cloud projection clustering, which are designed to reflect the properties of MLS-acquired point cloud. The algorithm first divides the data into small units according to the direction of the river. Second, the levee points are extracted by applying directional equalization and point cloud projection clustering. Finally, the levee point extraction was completed through a process of increasing accuracy through a test based on the levee design value. As a result of its application to the 1 km Anyang-cheon stream area, an urban river located in Seoul, Korea, the classification accuracy of 95.9 % was obtained. Also, the levee elevation was automatically calculated in 0.194 m and 0.13 m of mean absolute error (MAE) compared to manual and total station measurements, respectively.

1. Introduction

1.1. Levee management with digital twin

The risk of river flooding is increasing globally due to the frequent occurrence of heavy precipitation. In particular, damage caused by flooding may increase around urban river basins created as citizen-friendly spaces. Therefore, managing engineering structures constructed on the river is growing more critical to prevent river flooding. Levees are one of the most important engineering structures for protection against river flooding. As a facility installed on both sides of the river, the levee protects the residential area from flooding of river. A few cracks or losses of levee may lead to a significant levee collapse because

the levee is a linear structure. Excessive flow of river water due to the collapse of the levee can lead to a large-scale disaster. Therefore, it is important to monitor the physical properties of levees built over a considerable distance in detail. Especially for the earthen levee, a soil-compacted structure, continuous soil loss may occur due to a series of heavy rain events.

Digital twin refers to a virtual world built by copying multidimensional data from the real world. As it reflects properties of the real world in a virtual world, various simulation tests can be performed to establish a response manual for potential disaster events. As a result, decision-makers may have optimal solutions to tackle problems in the real world. In the case of river management, facility safety managers can monitor levees in multiple dimensions and conduct detailed safety

* Corresponding author.

E-mail address: sohn1@yonsei.ac.kr (H.-G. Sohn).

inspections. The safety inspection of the levee is based on the identification of the physical shape of the levee, such as lost inspection, levee slope inspection, and levee elevation inspection.

All this critical information can be provided through the construction of geospatial information-based digital twins.

Therefore, the digital levee twin needs to be built in an effective data format to grasp the physical shape of a levee. To this end, point cloud data acquired with a laser scanner was used as the base of the digital twin construction among several data forms (Jiang et al., 2021; Shanbari et al., 2016). Various laser scanner-based platforms such as TLS, ALS, and MLS are used to acquire point cloud data of the target. Point cloud represents the target as X, Y, and Z coordinate values. The expression ‘cloud’ means the physical shape of the target expressed in numerous points, which enables the detailed presentation of the target.

1.2. MLS LiDAR for levee mapping

The concept of a digital twin has historically attracted attention in urban research, but it was difficult to implement due to the lack of technology, operating environment, and infrastructure at that time. However, the realization of digital twin construction is emerging based on the technology advancement in communication, computation, and sensor devices (Rasheed et al., 2020). In particular, a modern data acquisition platform such as a vehicle-type MLS, which acquires data at high speed for a long time with high precision, enables periodical acquisition and update of data in a vast area (Choi et al., 2019). Existing geospatial data acquisition methods such as TLS, total station, and GNSS could also acquire high-precision data. However, a large temporal limit exists because data is obtained in a stop-and-go manner. This approach is not suitable for constructing a digital twin for facility monitoring.

In fact, it took about two weeks, including both data acquisition and post-processing, to build 500 m of geospatial data of the levee using the stop and go method, while vehicle-type MLS only took 10 min to acquire data for the same area (Lee et al., 2021). Research has also been conducted to quantitatively check changes in levees in a short time without installing reference points in the target area through an sUAS with a laser scanner (Akiyama et al., 2021). However, when laser scanners and cameras are combined, SUASs shorten their battery to tens of minutes. Also, there are strict regulations on flight permits and worries about possible damage in the event of a crash. Accordingly, the efficiency is significantly reduced in acquiring data for a large alignment such as a river. And since such an sUAS system has a flight coverage of only 2 km per flight, it is insufficient to inspect the entire 30,000 km river in the case of Korea.

For this reason, it is best to use vehicle-type MLS to build geospatial information-based digital twins. Despite its high cost and line of sight blockages in using a laser scanner, vehicle-type MLS can quickly and accurately acquire 3D geospatial data for a wide range in a short period. In addition, since it operates along the levee, it has the advantage of quickly grasping the longitudinal and crosssections of the levee.

1.3. Levee surface extraction from LiDAR

Various water-friendly facilities such as trees and sports facilities are installed on the levee of the river. These facilities act as obstacles while obtaining the physical shape of the levee because they may block the MLS signal arrival. Therefore, to grasp the levee’s exact shape, it is essential to remove objects other than the levee from the acquired geospatial data and leave only the levee data.

The process of extracting the physical shape of the levee is the same as generating a digital terrain model (DTM) by extracting ground points from the entire geospatial data. In this regard, various studies have been proposed on extracting bare ground points from geospatial information acquired through aerial laser scanners (ALSs) (Chen et al., 2017; Liu, 2008; Meng et al., 2010). Most methods using ALS data compare height, inclination angle, surface curvature, signal strength between adjacent

points (Axelsson, 2000; Evans and Andrew, 2007). Research to extract bare ground using ALS data can be divided into three categories: slope-based, morphology-based, and surface interpolation-based (Chen et al., 2016; Li et al., 2014; Liu, 2008; Mongus et al., 2014; Sithole and Vosselman, 2004). The slope-based study assumes that the points acquired on the ground have a gradient slope and extracts points with lower height values within the section as ground points (Vosselman, 2000). Morphology-based research performs classification assuming that the ground is flat (Błaszczański et al., 2015; Chen et al., 2007). The surface interpolation-based research performs classification assuming that the ground is a geometric plane expressed as a parameter (Błaszczański et al., 2015; Kraus and Pfeifer, 1998; Rapinski et al., 2011). Among the previous studies, the surface interpolation-based studies that better grasp the context show higher results than the others (Chen et al., 2016; Meng et al., 2010). However, these ALS-based data differ from MLS-based data in terms of the geometry of data acquisition, point density, and point characteristics (Che et al., 2019; Olsen, 2013; Pirotti et al., 2013; Rodríguez-Caballero et al., 2016). Therefore, due to the different characteristics between ALS and MLS, there is a limit to applying ALS-based studies directly to MLS datasets (Che et al., 2019; Meng et al., 2009; Olsen, 2013; Rodríguez-Caballero et al., 2016; Sithole and Vosselman, 2004; Wang et al., 2009).

Therefore, ground extracting methods from MLS-acquired data have been devised. The methods can be grouped into three major categories: rasterization-based, 3D-based, and scanline-based (Che et al., 2019). The rasterization-based method processes 3D point cloud data by rasterizing it in 2D according to various characteristics such as intensity. Through rasterization, a wide variety of image processing techniques can be utilized in handling 3D data (Chen et al., 2021; Jung et al., 2019; Serna and Marcotegui, 2014, 2013; Yang et al., 2012). Also, the computational load would reduce because the 3D data is compressed into 2D pixels. However, the detailed information of the data may be lost simultaneously.

In 3D-based methods, the 3D data is utilized in original format to preserve the details. Because of the complexity of the data, researchers are interested in dividing the data into a 2D square grid and utilizing the distribution of Z values (Husain and Vaishya, 2016; Lin and Zhang, 2015; Yadav et al., 2017). Alternatively, the data is handled by converting it into 3D voxels (Ibrahim and Lichti, 2012; Yu et al., 2015). Along with the improvement of computational power, such as GPU development, research on 3D-based methods is becoming active.

In scanline-based methods, the point cloud data is broken down into sets of scanlines based on GNSS acquisition time or laser acquisition angle (Che and Olsen, 2017; Teo and Yu, 2015; Wu et al., 2016). Through the methods, it is possible to increase data processing efficiency and reflect the characteristics of data acquisition by the laser scanners.

However, data occlusion may be inevitable when constructing data in a real-world environment due to limited accessibility. In particular, in the case of the levee, the data acquisition is often conducted only on either the land side or the river side of the levee. The existing algorithms could not effectively extract the levee surface using vehicle-type MLS data. Therefore, the researchers devised an algorithm that can effectively extract the levee surface, even using data acquired only from one side of the levee.

Accordingly, this study proposed a new algorithm for extracting the levee surface from the point cloud acquired through MLS. The proposed algorithm uses the data acquisition direction of MLS and the distribution aspect of the levee point cloud. The proposed algorithm can be easily used for safety checks for flood prevention by measuring the height and slope of the levee, identifying changes in the levee, and small-scale collapse areas of the levee.

2. Materials and methods

2.1. Data acquisition

2.1.1. MLS for rivers

MLS equipment was initially designed to construct geospatial information for road facilities while driving through cities. It is applicable for facilities distributed in a long and wide space, such as continuous roads and rivers. The MLS used in this study comprises cameras, laser scanners, and GNSS/INS mounted on a small electric vehicle. It can operate on a bicycle path along a river to provide full access to river facilities. The sensors in the MLS for rivers are synchronized in time and space to acquire comprehensive data as the vehicle moves along the river. The final form of the data obtained contains both location and three-dimensional shape information, called a point cloud, in every single frame.

Fig. 1 (a) shows the MLS used for data acquisition, and **Fig. 1** (b) shows the point cloud in panoramic view. As indicated in **Table 1**, our MLS consists of two laser scanners, four cameras configured to acquire 360° images, and a single GNSS/INS sensor; the system was well calibrated before collecting data sets. The research utilized X, Y, Z, and intensity information only, not RGB.

2.1.2. Study area

Anyang-cheon was selected as the study area. It is a representative urban river managed by the Ministry of Land, Infrastructure, and Transport (MOLIT) and the Seoul Metropolitan Government. Anyang-cheon flows 34.8 km from Anyang, Gyeonggi-do, a city in the southwestern part of Seoul, and joins the Han River in Seoul. **Fig. 2** shows Anyang-cheon marked in red; the Seoul metropolitan city borders are denoted by a yellow line.

According to the basic river plan, which is the standard document for maintaining Korean national rivers such as Anyang-cheon, MOLIT established cross-sectional survey lines at intervals of 250 m for the river and conducted surveys using a total station and GNSS in 2015. The survey lines were segmented into 20 survey areas in the downstream direction and managed by naming them in the form of “site no. + distance (less than 1,000 m)” from the start point of each area (MOLIT, 2015). For each survey line, representative design values, such as the design flood level and freeboard standard according to design flood discharge, were suggested in preparation for 100-y flood events. The design levee elevation was measured as the summation of the freeboard standard and design flood level. Here, the design levee elevation is the elevation value that the levee is expected to maintain despite post-construction deviations such as natural settlement. **Table 2** presents the representative design values (MOLIT, 2018, 2015). The calculated design levee elevation was used to test and evaluate the accuracy of the proposed algorithm. In this study, detailed data were obtained using

Table 1

Specifications of mobile laser scanner (MLS) components.

Equipment	Model	Specifications
LiDAR	1 Velodyne Ultra puck (front)	<ul style="list-style-type: none"> - 32-channel - Laser precision: up to ± 3 cm - Horizontal FOV: 180° - Vertical FOV: -15°–25° - Frequency: 5–20 Hz - Effective range: up to 200 m - ~1,200,000 points per second
	1 Velodyne puck (rear)	<ul style="list-style-type: none"> - 16-channel - Laser precision: up to ± 3 cm - Horizontal FOV: 180° - Vertical FOV: -15°–15° - Frequency: 5–20 Hz - Effective range: up to 200 m - ~600,000 points per second
Cameras	4 Canon DSLR	<ul style="list-style-type: none"> - FOV: 82.4° × 66.9° - Focal length: 5 mm - Camera sensor format: 2/3"- Resolution (megapixels): 5.00 - Pixels (H × V): 2,448 × 2,048- Max. frame rate (fps): 35 - Pixel depth: 12 bit
GNSS/INS	1 pwrPAK7-E1	<ul style="list-style-type: none"> Position accuracy (m)- Horizontal: 0.01 (post-processed), 0.02 (RTK)- Vertical: 0.02 (post-processed), 0.03 (RTK) Attitude (°)- Roll: 0.005 (post-processed), 0.015 (RTK)- Pitch: 0.005 (post-processed), 0.015 (RTK)- Heading: 0.017 (post-processed), 0.035 (RTK)

MLS for a 1 km portion of the Anyang-cheon basin covered by five survey lines from No.12 + 927 to No.13 + 656.

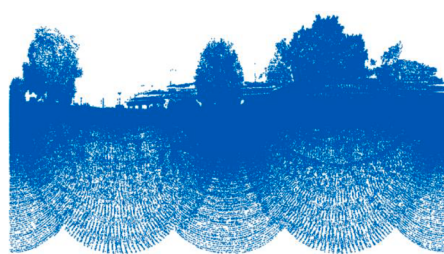
The point cloud was acquired while driving the MLS at a speed of less than 20 km/h, which is the national standard for safe travel on bicycle paths along the river. It took 5 min to collect 25,582,039 three-dimensional points covering 1 km of the river. The approximate locations of the survey lines in the study area are displayed on the aerial image in **Fig. 3**. The figure also shows the point cloud (marked in red and orange) projected over the study area.

2.1.3. LiDAR data accuracy assessment

The accuracy of the data acquired by the MLS was evaluated by comparing the values of the check points to those obtained with the TLS and GNSS, as shown in **Fig. 4** (Hong et al., 2017). **Fig. 4** (a) and (b) show check points of the data acquired with the MLS and TLS, respectively. The results confirmed that the MAEs were 0.09 m in 2D and 0.161 m in 3D. And the mean absolute residual based on a flat segment-based



(a)



(b)

Fig. 1. (a) Mobile laser scanner equipment (MLS) for rivers used in this study; (b) Acquired LiDAR data in panoramic view.

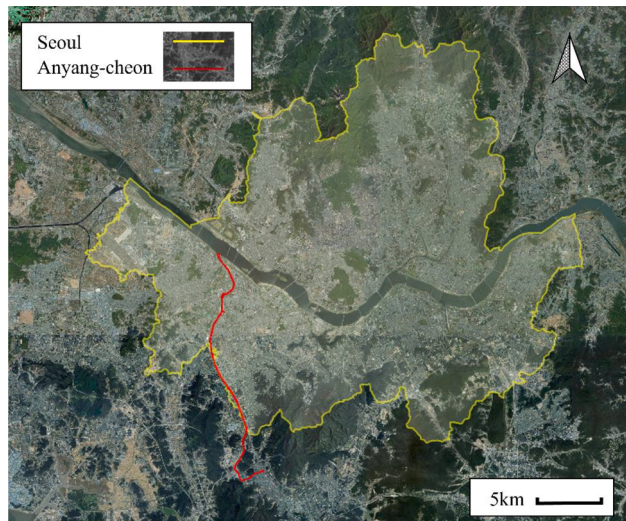


Fig. 2. Anyang-cheon and the Seoul metropolitan city borders.

Table 2

Design levee elevations along the survey lines.

Survey line (No. + meter)	Design flood discharge (m ³ /s)	Freeboard standard (m)	Design flood level (m)	Design levee elevation (m)
12 + 927	1,620	1 m	39.568	39.568
13 + 166	1,620	1 m	39.715	39.715
13 + 185	1,620	1 m	39.731	39.731
13 + 407	1,620	1 m	39.871	39.871
13 + 656	1,620	1 m	39.871	39.871

precision test was 0.011 m.

2.1.4. Automatic levee elevation estimation

Fig. 5 shows the schematic workflow of the algorithm for automatic levee elevation estimation based on the point cloud data. The algorithm initially extracts the levee point cloud from the original input point cloud and then measures the levee elevation. The algorithm consists of three main processes.

First, the point cloud was broken into 10 m segments based on the GNSS epoch interval. This helps the algorithm to gain advantages in computational efficiency and processing time. Also, the segmentation acts as a mathematical linearization for curved levee alignment so that the proposed methods work well for linear and nonlinear surfaces. Here, a segmented unit point cloud refers to a point cloud segmented in the unit of the GNSS epoch. In our case, the geospatial interval of the GNSS epoch was set to 10 m of MLS movement. The original point cloud in the transverse Mercator (TM) coordinate system is rotated parallel to the local coordinate system of the MLS. This coordinate transform helps conduct segmentation of the input point clouds and facilitates the processing of subsequent steps. The final product of the first process is a segmented unit point cloud according to each GNSS epoch.

The second process extracts “the levee surface” from each segmented unit point cloud. The levee point cloud refers to only the levee portion of the segmented unit point cloud. The process is applied to each segmented unit point cloud and consists of three steps. In the first step, the levee point cloud is selected from the segmented unit point cloud using directional equalization. Directional equalization removes the non-levee point clouds by equalizing point coordinates in a vehicle-moving direction. In the second step, projective clustering is performed on the extracted levee point clouds obtained in the first step. Projective clustering enhances the performance of existing density-based clustering. The third step checks whether there are errors in the



Fig. 3. Aerial photograph of the study area and survey lines with point cloud projection.

previous processes and corrects them. Error checking is performed by a simulation test based on the design levee elevation provided in the river basic plan, and complementary clustering follows the test result. With the completion of all three steps, levee point clouds are extracted from each segmented unit point cloud.

The third process estimates levee elevations from the segmented unit levee point clouds. The final levee point cloud can be obtained by rearranging every levee point cloud along the GNSS epoch. Each of the three major processes is explained in detail in the following sections.

2.2. Unit point cloud segmentation based on GNSS epoch

It is critical to find a river area and specify the levee area based on extensive data acquired by acquisition methods such as ALS, and research has been actively conducted (Casas et al., 2012; Saye et al., 2005). When using MLS for river facility surveying, data are obtained while the vehicle is moving along the levee. In this context, the movement direction of the MLS can be assumed to be the direction of the river flow. Under this assumption, the movement direction vector of MLS, \vec{v}_i , can be calculated for each epoch of the GNSS as the difference between two position vectors representing the MLS position at epoch i and $i + 1$, as shown in Eq. (1). Here, g_i and g_{i+1} represent the GNSS point vectors at epochs i and $i + 1$, respectively.

$$\vec{v}_i = g_{i+1} - g_i \quad (1)$$

The MLS obtains GNSS data on the longitude-latitude coordinate system in the World Geodetic System (WGS84) ellipsoid. The data are converted to the TM coordinate system, which consists of the northing (N), easting (E), and ellipsoidal height (h), as shown on the left side of Fig. 6. Because the levee elevation data are based on the geoid, the ellipsoidal height is converted into orthometric height (Z) using the

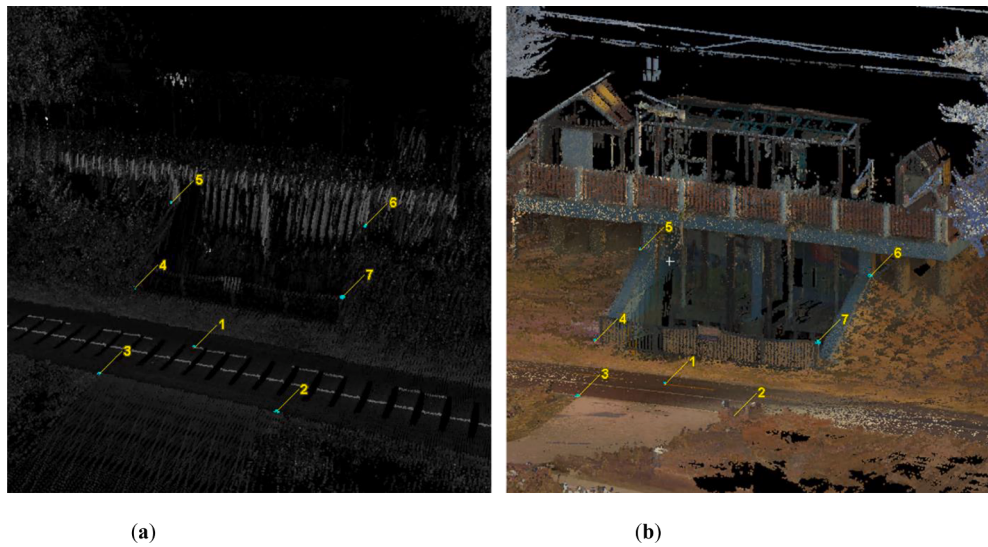


Fig. 4. Check points for MLS accuracy. (a) Check points on MLS data, (b) Check points on georeferenced TLS data.

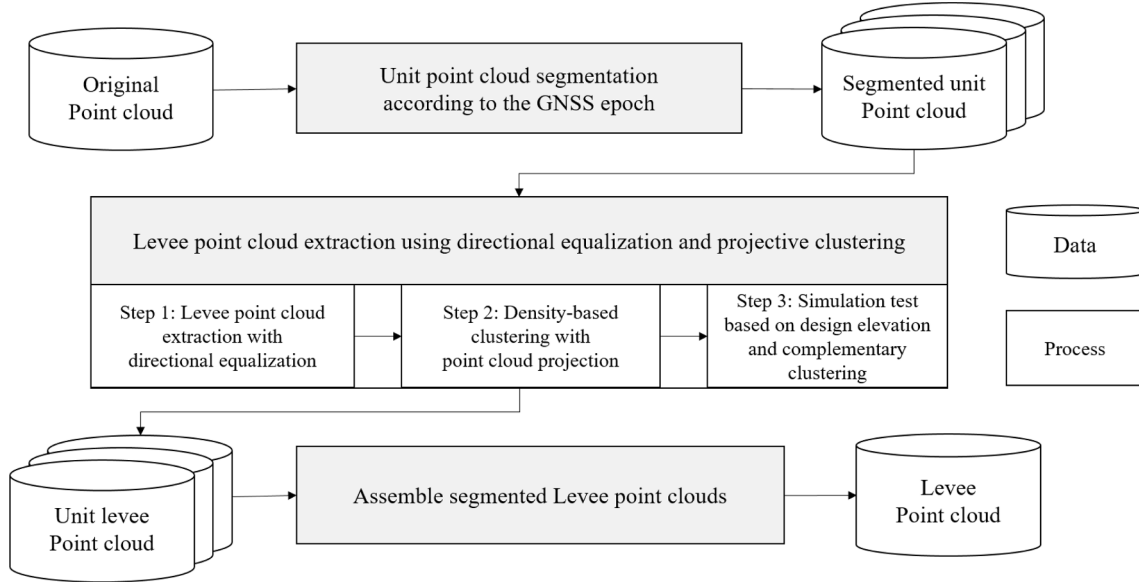


Fig. 5. Schematic workflow for automatic levee extraction estimation.

Korean geoid model (Lee et al., 2011). To facilitate the subsequent algorithms, the point cloud data in the TM coordinate system were transformed into the local MLS coordinate system (X^L , Y^L , Z^L) at each GNSS epoch. The positive direction of the local X-axis corresponds to the direction of the MLS movement, i.e., \vec{v}_i . The positive direction of the local Z-axis corresponds to the opposite direction of the plumb line, and the local Y-axis completes the right-handed coordinate system along the levee, as shown on the right side of Fig. 6.

This transformation from the TM coordinate system to the local MLS coordinate system proceeds from GNSS epoch $i = 1$ to the final epoch, $i = 100$. The rotation matrix for each epoch is calculated using Eqs. (2)–(6) from Rodrigues' rotation formula:

$$R_i = I + \left[\vec{a}_i \right]_x + \left[\vec{a}_i \right]_x^2 (1 - c_i)/s_i^2 \quad (2)$$

$$\left[\vec{a}_i \right] = \begin{bmatrix} 0 & -a_{i3} & a_{i2} \\ a_{i3} & 0 & -a_{i1} \\ -a_{i2} & a_{i1} & 0 \end{bmatrix} \quad (3)$$

$$\vec{a}_i = \vec{v}_i \times \vec{x} \quad (4)$$

$$s_i = \| \vec{a}_i \| \quad (5)$$

$$c_i = \vec{v}_i \bullet \vec{x} \quad (6)$$

where I is a 3×3 identity matrix; \vec{x} is $(1, 0, 0)$; \vec{a}_i represents the cross product of \vec{x} and \vec{v}_i in Eq. (1); s_i represents the norm of \vec{a}_i , which is the sine value between \vec{v}_i and \vec{x} ; and c_i represents the scalar product of \vec{v}_i and \vec{x} , which is the cosine value between \vec{v}_i and \vec{x} . Through this rotation, the original point cloud in the TM coordinate system is transformed into the local MLS coordinate system. The transformed point cloud is segmented into unit point clouds according to the GNSS epoch in the direction of the local X axis.

2.3. Directional equalization and projection clustering of MLS data

Various methods have been proposed to distinguish levee points from non-levee points in the original point cloud to create a DTM

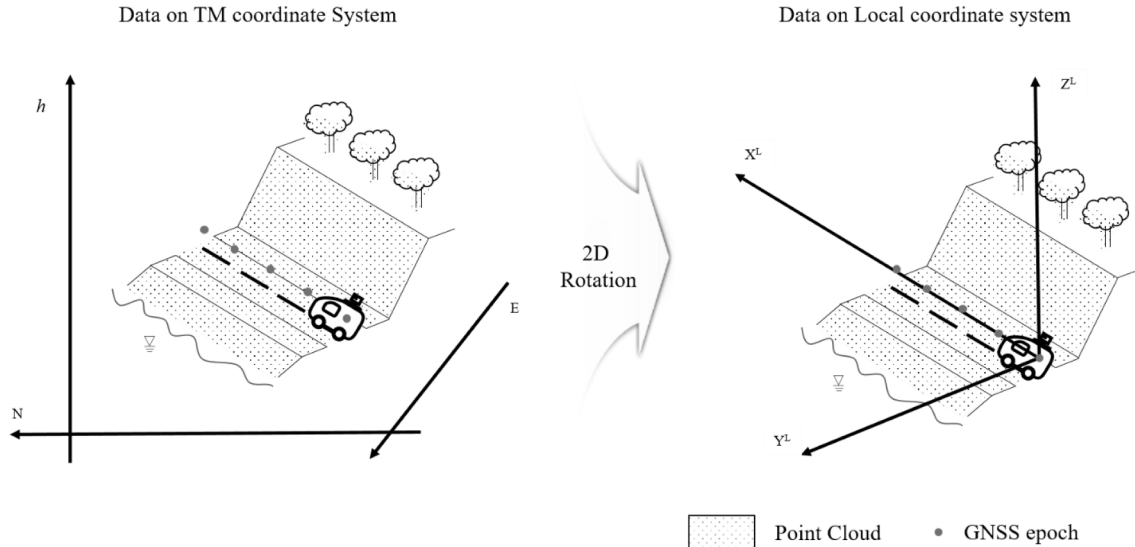


Fig. 6. Coordinate transformation of the acquired MLS data.

(Kobler et al., 2007; Kraus and Pfeifer, 1998; Liu, 2008; Mongus et al., 2014; Zhang et al., 2016). However, there is a limitation to straightforwardly applying algorithms developed for ALS to MLS (Cai et al., 2018; Gézero and Antunes, 2017; Tyagur and Hollaus, 2016; Vallet and Papelard, 2015). ALS is designed to look down toward the ground, whereas MLS has a side-looking system. In the ALS case, the levee point indicates the lowest point based on the Z value in the predefined kernels in the XY plane. As shown on the left side of Fig. 7, the levee points can be extracted by selecting the lowest Z values within the kernel in the ALS data.

For MLS data, however, selecting the lowest point within the predefined kernels may not always match the levee points owing to the characteristics of the MLS. As shown on the right side of Fig. 7, some extracted points within the kernels do not correspond to the actual levee in locations, especially at the most faraway points from the MLS sensors. This is because MLS looks at objects from the side of the ground (Che et al., 2019; Olsen, 2013). This situation is unavoidable when operating an MLS along the bicycle path near the levee. To resolve these issues, we proposed the following techniques to extract the levee points from the

MLS-acquired data.

2.3.1. Levee point cloud extraction with directional equalization

As discussed above, at this point, the acquired data is in the state of segmented unit point clouds along the direction of MLS movement, as shown in Fig. 8 (a). To extract the levee points and avoid obstacles, directional equalization was proposed. Directional equalization is a method for equally distributing the points of the segmented unit point clouds along the MLS movement direction. Fig. 8 (b) shows the conceptual result of the segmented unit point cloud with directional equalization. Fig. 8 (c) shows the result of the levee point extraction applied to the equalized segmented unit point cloud.

Directional equalization prevents the lowest part of the obstacle point cloud from being considered a levee point. As a result, even if the obstacle point in the area has the lowest Z value instead of the levee point owing to blockage by an obstacle, the levee point cloud acquired in the adjacent area in the X-axis direction is arbitrarily drawn under the obstacle points. The arbitrarily drawn levee points prevent the obstacle points from being incorrectly extracted as levee points because they will

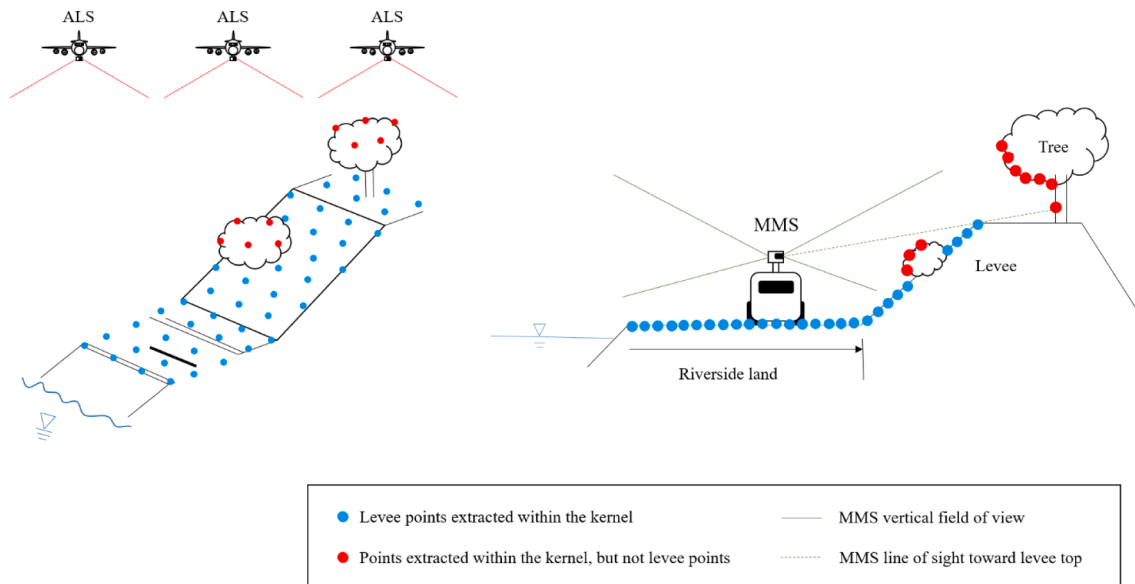


Fig. 7. Comparison of levee point cloud extraction results for data acquired with ALS (left) and MLS (right).

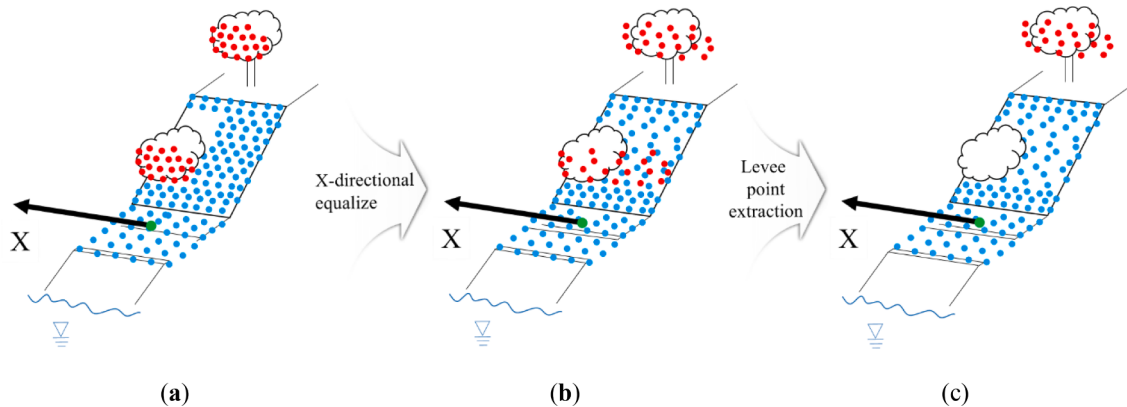


Fig. 8. Schematic diagram of X-direction equalization and levee point extraction, red points represent points which should be removed, and blue points represent levee points. (a) original segmented point cloud, (b) the conceptual result with directional equalization, (c) after levee point extraction. (For interpretation of the references to color in this figure legend, the reader is referred to the web version of this article.)

have the lowest Z value in the corresponding kernel instead of the obstacle points.

Directional equalization is performed according to Eqs. (7)–(8). Eq. (7) represents the i th segmented unit point cloud, which contains n points with (X, Y, Z) coordinates, as displayed in Fig. 8 (a). When directional equalization is applied along the X axis, the X values are replaced with equalized values between the X values of the i th GNSS point and $(i+1)$ th GNSS point, which are the starting and ending points of the i th segmented unit point cloud. Eq. (8) represents the segmented unit point cloud with X-directional equalization, and X_{eq}^i ($1 \leq j \leq n$) represents the X values randomized in the range of x_j^i ($1 \leq j \leq n$).

$$P^i = [X^i Y^i Z^i] = \begin{bmatrix} x_1^i & y_1^i & z_1^i \\ x_2^i & y_2^i & z_2^i \\ \vdots & \vdots & \vdots \\ x_n^i & y_n^i & z_n^i \end{bmatrix} \quad (7)$$

$$P_{x_eq}^i = [X_{eq}^i Y^i Z^i] = \begin{bmatrix} x_{eq_1}^i & y_1^i & z_1^i \\ x_{eq_2}^i & y_2^i & z_2^i \\ \vdots & \vdots & \vdots \\ x_{eq_n}^i & y_n^i & z_n^i \end{bmatrix} \quad (8)$$

After applying directional equalization, the segmented unit point

cloud is further segmented into small kernels based on the X and Y coordinates. For each point cloud within each kernel, points within a specific range of Z values are extracted as the levee point cloud. The particular range of Z values starts from the lowest Z value and ends at the lowest value plus a Z-threshold value. As the size of the kernel decreases, the lower part can be extracted without losing the original data. However, it is recommended that the ratio between the Z value range and the Y length of the grid follow the levee slope criterion in the basic river plan, which should not exceed 1/2 (Choung, 2014; MOLIT, 2015, 2018). When the ratio is less than this criterion value, a part of the levee point cloud may be lost; in the opposite case, too many points may be extracted as the levee point cloud. In the experiment conducted in this study, the X and Y lengths of the kernel were set to 0.4 m, and the Z value range was set to 0.2 m to ensure the ratio between the Z value and a side of the square grid did not exceed the levee slope criterion. After extracting the levee points, the X values of each extracted levee point cloud are rolled back to obtain the original values, following the index defined before equalization.

2.3.2. Density-based clustering with point cloud projection

After extracting the levee point clouds through Step 1, as shown in Fig. 9 (a), non-levee point clouds were still extracted as levee point clouds because Step 1 can only remove non-levee point clouds that are overlaid to levee surface. These remaining non-levee point clouds, which do not have nearby levee point clouds, appear to be floating in

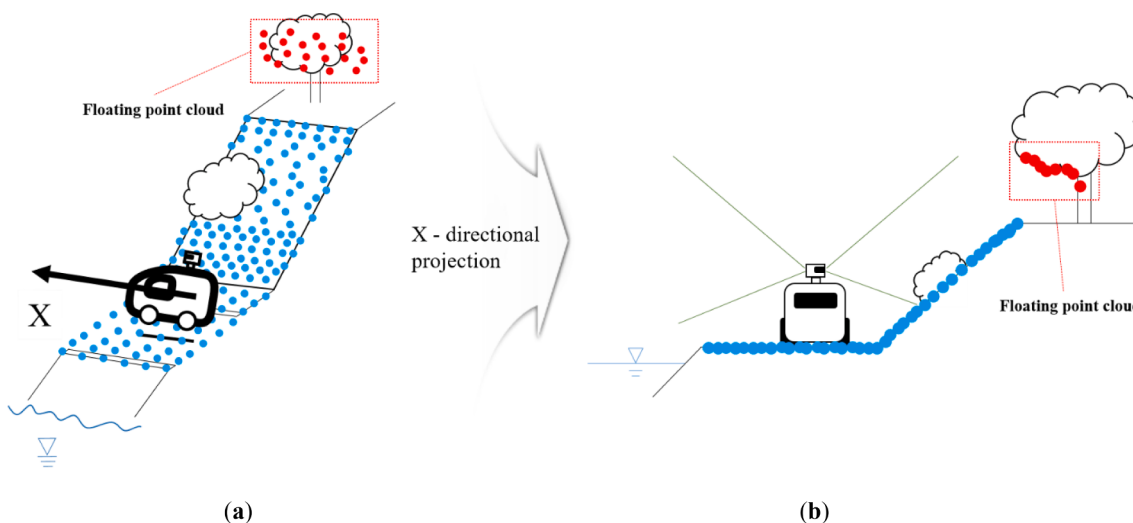


Fig. 9. Schematic diagram of X-direction projection.

space. Therefore, these remaining non-levee point clouds are referred to as floating-point clouds. In *Step 2*, density-based clustering with point cloud projection is applied to remove the floating-point clouds.

Typically, the points constituting the point cloud are clustered at a high density. Therefore, the distance between points in the same point cloud is shorter than the distance between different point clouds. As a result, it is appropriate to use density-based clustering to distinguish each point cloud: in this case, the floating-point clouds and the levee point clouds. Furthermore, to increase the clustering performance, point cloud projection on the X and Y axes is applied as a preprocessing step.

Density-based clustering analysis is a clustering technique that defines points within a given radius from a specific location as one cluster (Kriegel et al., 2011). There are several types of density-based cluster analysis techniques, and the density-based spatial clustering of applications with noise (DBSCAN) algorithm is used in this study. The DBSCAN algorithm starts its process from a random point that has not been visited and searches for the existence of points within a radius of ϵ . If points exist around the starting point, then these are added as a cluster and marked as visited. The clustering continues until there are no additional neighboring points inside the radius ϵ . A new unvisited point outside the cluster then becomes the new starting point, and the process is repeated until all points are marked as visited. DBSCAN is suitable for clustering point clouds because it requires few parameters and is specialized for clustering datasets with geometric distributions (Ester et al., 1996).

However, when DBSCAN is applied to point cloud data obtained from an actual environment rather than a desirable data environment, clustering may not be conducted as intended because the point cloud is scattered by obstacles. Therefore, as shown in Fig. 9 (b), point cloud projection is applied in both parallel and vertically in the X direction to increase the effect of clustering. With this point cloud projection, the dimension of the distance calculation between points is reduced from three to two dimensions. Moreover, the density values of point clouds of the same type increase, enabling finer clustering with a smaller search range (ϵ) to obtain better results. In particular, because the MLS movement direction and the direction in which the levee is constructed are the same, the projection of the MLS toward the movement direction is effective for removing floating points while minimizing the loss of the levee point cloud, as shown in Fig. 9 (b). After distinguishing the levee point cloud by point projection along the movement and DBSCAN, projections in the vertical direction of the movement and DBSCAN are performed as a second clustering. Because the floating-point cloud is floating in the Z-axis direction, projection toward the Z-axis, which removes the Z value difference, has no positive effect on clustering. Therefore, only two projections were applied, excluding the Z-axis projection.

2.3.3. Simulation test based on the design elevation and complementary clustering

To evaluate the result of *Step 2* and complement the extraction, *Step 3* compares the levee elevation measured from the extracted levee point cloud to the design levee elevation listed in Table 2. The levee elevation was measured by checking the Z values of the extracted levee point cloud. If the error between the levee elevation measurement and the design elevation in the basic river plan was larger than the threshold, the result of *Step 2* was defined as a candidate for misclassification.

Specifically, when the value obtained by subtracting the design height from the levee elevation measurement is less than the negative threshold, it indicates that more parts were classified as non-levees during *Step 2*. Therefore, clustering was performed again on the non-levee point cloud, and the cluster in which the Z value represents the lowest value was included as the levee point cloud. The positive case indicates that more point clouds were classified as levee point clouds than the actual levee. Clustering was then performed on the levee point cloud to exclude clusters with high Z values. This is based on the premise that there is no significant difference greater than the threshold between

the design elevation and the measured levee elevation unless a serious natural disaster occurs. For the period in which Anyang-cheon has been continuously and systematically managed since 1991, this assumption seems to be reasonable. The threshold value was set to 1 m. The result of *Step 3* is a unit levee point cloud extracted from each segmented unit point cloud. The levee elevation for each unit levee point cloud is measured for the final estimation. The levee elevation is calculated for each GNSS epoch. The unit levee point clouds extracted for each segmented unit point cloud are rearranged along the GNSS epochs, which are the standards for segmentation. Through this process, the extraction of the entire levee point cloud was completed.

3. Results

This section shows the results of applying the above-mentioned processes and steps sequentially to the actual data. The experiment was conducted with an Intel i5-10400F CPU and a GTX 1050ti GPU in the Windows 10 operating system using MATLAB as the programming language. Figs. 10 and 11 show the results of the first process and unit point cloud segmentation according to the GNSS epoch, respectively.

The rotation and segmentation processes of the point cloud are shown in Fig. 10. Fig. 10 (a) shows the data in the TM coordinate system; the arrow indicates the MLS movement direction in time sequence i with vector \vec{v}_i according to the GNSS epoch. Fig. 10 (b) shows the results of the point cloud rotation. The arrow \vec{v}_i represents vector $(1, 0, 0)$, which means that the MLS movement direction in the original TM coordinate becomes the X-axis in the new coordinate system. Through this rotation, the point cloud segmentation could be smoothly conducted, as shown by the green points in Fig. 10 (b). Fig. 11 (a) shows the segmented unit point cloud according to GNSS epoch, i . Fig. 11 (b) shows a cross-sectional view of the segmented unit point cloud.

Figs. 12–14 show the results of *Step 1* of the second process: levee point cloud extraction with directional equalization. Fig. 12 (a) shows the segmented unit point cloud data, in which only part of the levee was acquired because of obstacles such as bushes. As shown in Fig. 12 (a), when obstacles were present, the geospatial data of the obstacles were acquired instead of the levee point cloud of the area. Through directional equalization, the levee point cloud partially acquired in the adjacent area without obstacles was extended to the area covered by obstacles located under the obstacle point clouds. Fig. 12 (b) shows the resulting point cloud after directional equalization. As shown in Fig. 12 (b), directional equalization could be performed with less computational load after applying rotational transformation with the MLS movement direction as the X axis.

Fig. 13 shows the results of the levee point cloud extraction on the segmented unit point cloud with and without directional equalization. As shown in Fig. 13 (a), when directional equalization was used, the levee points extended by the directional equalization prevented the lowest point clouds of obstacles from being extracted as levee points. Fig. 13 (b) shows the extraction results without directional equalization, in which the lower points of the obstacles were misclassified as levee points.

Fig. 14 shows the superimposed results of Fig. 13, which clearly shows the misclassification of data according to the application of directional equalization. The extracted levee points with directional equalization are displayed according to their point intensity (mostly blue), whereas the lowest points from obstacles are displayed in red.

Fig. 15 shows the results of *Step 2* of the second process: density-based clustering with point cloud projection. The figures represent the original point cloud, each intermediate product, and the final result. Fig. 15 (a) shows the levee point clouds extracted after the previous processes. Clustering results according to the projection direction are depicted sequentially in Fig. 15 (b) and (c), where each cluster is represented by a different color. The most dominant clusters were extracted as the levee point cloud, and the final result is presented in Fig. 15 (d).

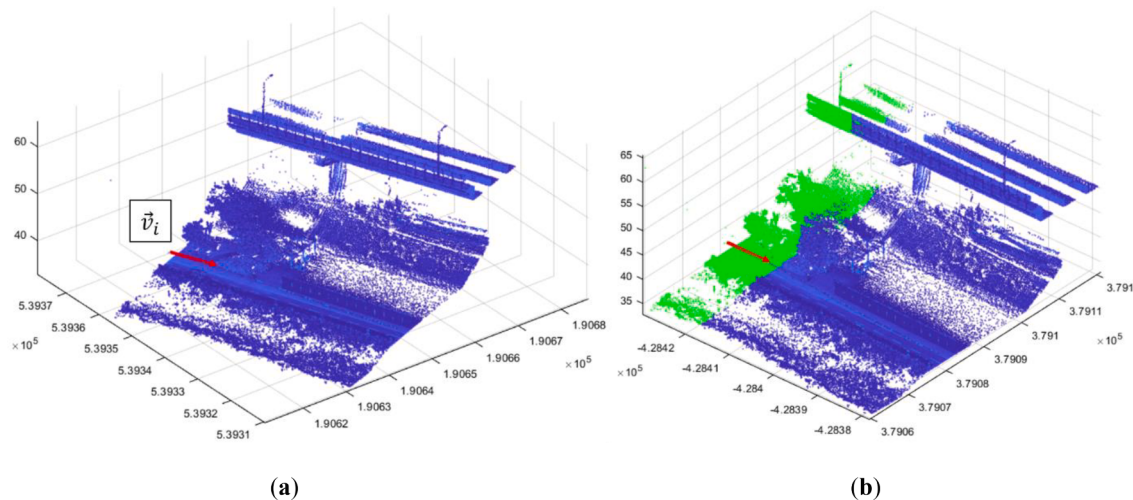


Fig. 10. (a) Part of the point cloud data and MLS movement direction vector at time sequence i in the TM coordinate system; (b) rotated point cloud and segmented unit point cloud colored in green. (For interpretation of the references to color in this figure legend, the reader is referred to the web version of this article.)

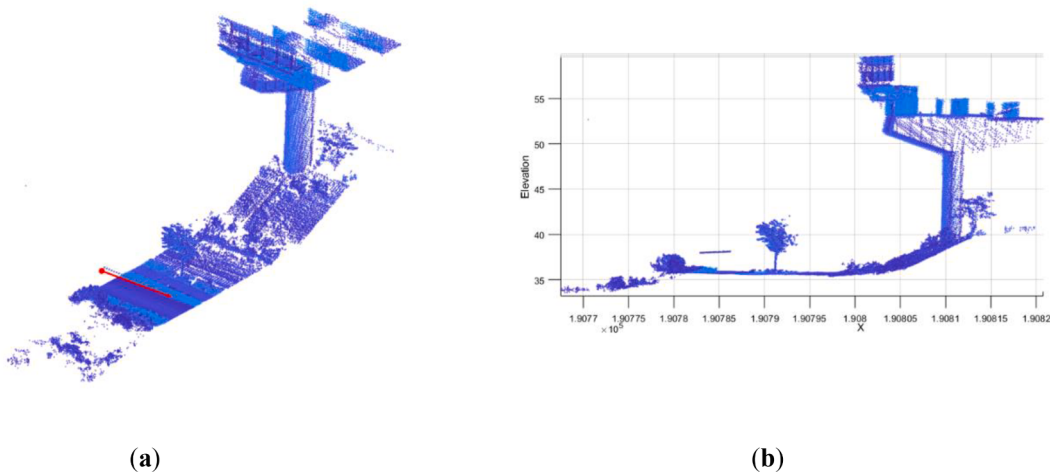


Fig. 11. (a) Segmented unit point cloud according to the GNSS epoch with a vector arrow representing the MLS movement direction; (b) cross-sectional view of the segmented unit point cloud.

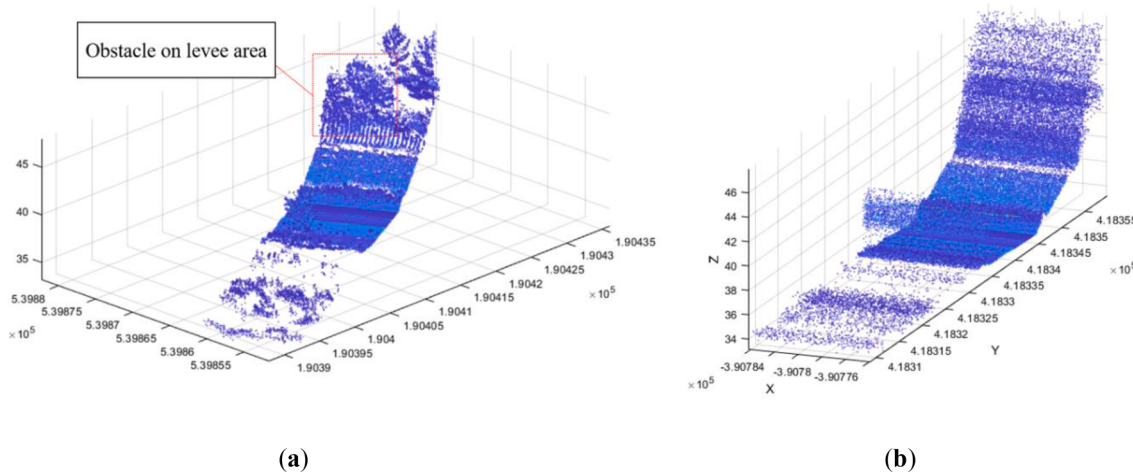


Fig. 12. (a) Example of a segmented unit point cloud in which the levee data are partially acquired owing to obstacles; (b) result of directional equalization on the example segmented unit point cloud.

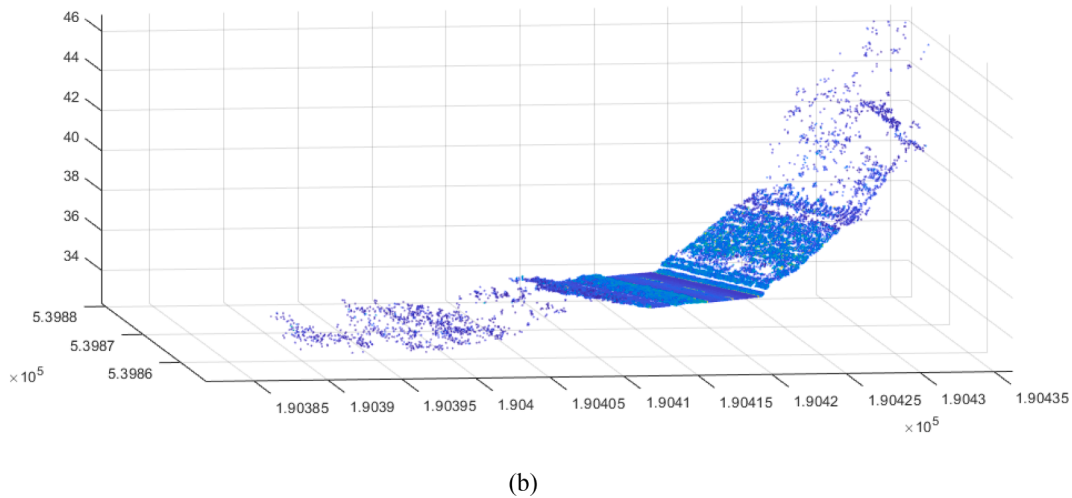


Fig. 13. Comparison of the results of levee point cloud extraction (a) with directional equalization, and (b) without directional equalization.

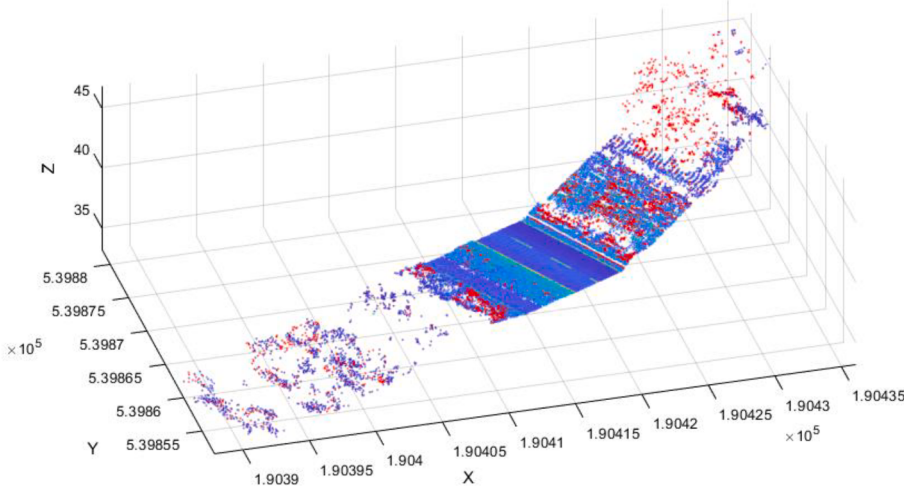


Fig. 14. Comparison of the levee point cloud extraction results with and without directional equalization in a single plot image.

Fig. 16 shows the actual results of Step 3 of the second process: a simulation test based on design elevation and complementary clustering. **Fig. 16** (a) shows the negative case, in which the measurement of the levee elevation was lower than the design levee height. The green points are the points added by complementary clustering. On the other hand, **Fig. 16** (b) shows the positive case, in which the measurement of the levee elevation was higher than the design levee height. The red points were over-extracted and removed through complementary clustering.

Fig. 17 shows the result of the final process: assembly of segmented levee point clouds. The original point cloud is displayed according to its intensity, and the point cloud of the extracted levee is displayed in green. The entire process took 10,274 s.

4. Discussion

4.1. Comparison with the manually obtained levee point cloud

The accuracy of the proposed method was evaluated by comparing the extracted levee point cloud result and the ground truth point cloud for an 1 km alignment. Ground truth point cloud was extracted manually from the entire point cloud using Cyclone, a point cloud editing program by Leica-geosystems. The results obtained by the proposed method were also compared with other filtering algorithms that can be used for non-

profit purposes such as LAStools, cloth simulation filtering, and simple morphology filtering. LAStools is a software developed by rapidlasso GmbH which can be operated in representative GIS programs such as QGIS and ArcGIS. LAStools provides a tool for ground filtering using point clouds named Lasground_new based on the adaptive triangulated irregular network (ATIN) algorithm. Users can set some parameters such as terrain type and a resolution for pre-processing for triangulated irregular network (TIN) creation. Among the various combinations of parameters, the two-parameter pairs with the highest result accuracy (terrain type = nature, preprocessing = hyper fine) and (terrain type = city, preprocessing = hyper fine) were selected as representative results. In addition, two algorithms, simple morphological filter algorithm (SMRF) and cloth simulation filtering (CSF), were used, and the results with the best accuracy were also selected for comparison. The parameters utilized are (grid resolution = 1) for SMRF. (rigidness = city area, isSmooth = 1, clothResolution = 0.5, max_iteration = 500 and class_threshold = 2) for CSF. Also, the projective clustering was applied to each resulting levee point cloud after the filtering to remove the outliers.

For accuracy evaluation, indicators used to evaluate the accuracy of the classification model were used, as shown in Eqs. (9)-(13) and **Table 3**. Accuracy tells how much the classified point cloud matches the actual point cloud. Precision is the proportion of point clouds classified as levee, actually representing levee. Recall is the proportion of point clouds classified as levee by algorithms among actual levee point clouds.

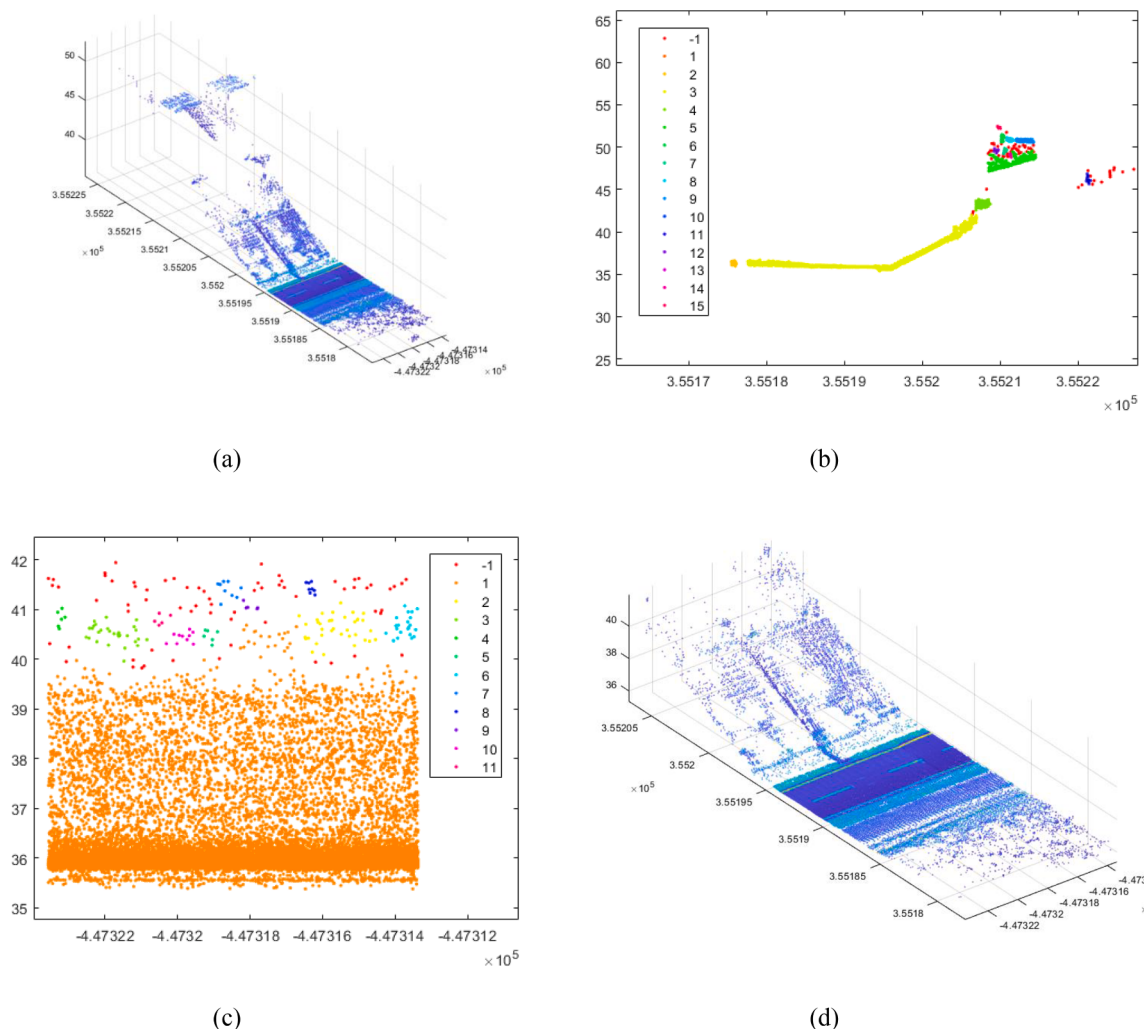


Fig. 15. Process of density-based clustering with point cloud projection: (a) levee point clouds before the process; (b) clustering result after the first projection along the MLS movement direction; (c) clustering result after the second projection vertical to the MLS movement direction; (d) final result of the levee point classification.

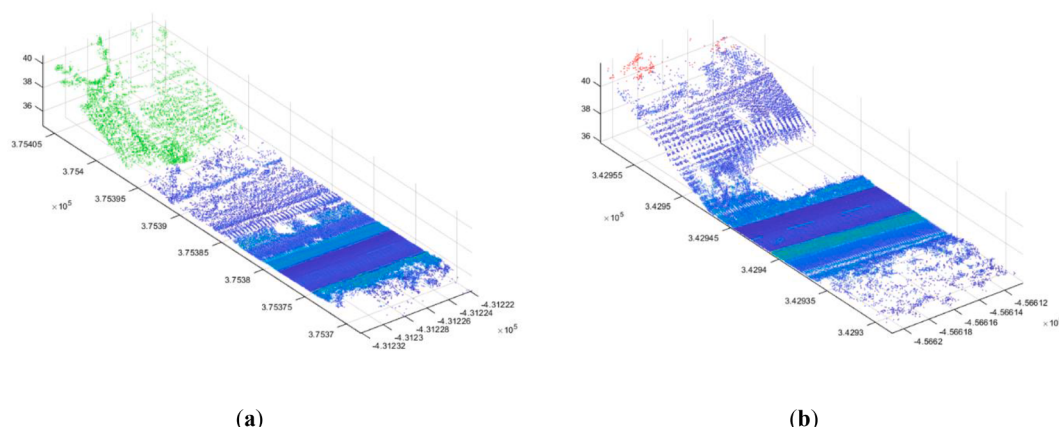


Fig. 16. Results of complementary clustering: (a) negative error, in which the green points are added to the points displayed according to the intensity; (b) red points are removed points. (For interpretation of the references to color in this figure legend, the reader is referred to the web version of this article.)

Fall-out refers to the rate at which point clouds, non-levee points, are misclassified as a levee. F1 score means the harmonic mean of precision and recall. Table 3 shows the results of the accuracy evaluation on each method.

$$\text{Accuracy} = \frac{TP + TN}{TP + TN + FP + FN} \quad (9)$$

$$\text{Precision} = \frac{TP}{TP + FP} \quad (10)$$

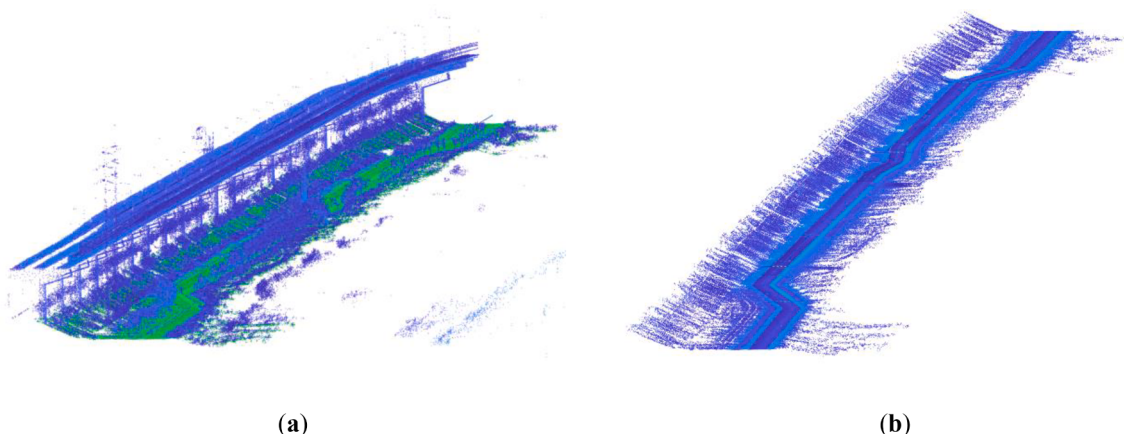


Fig. 17. Final levee extraction results; (a) the original point cloud is displayed according to its intensity (mostly blue), and point cloud of the extracted levee is displayed in green, (b) the levee point clouds displayed according to the intensity. (For interpretation of the references to color in this figure legend, the reader is referred to the web version of this article.)

Table 3
Assessment result (%).

Methods	Accuracy	Precision	Recall	Fall-out	F1 score
LAStools_nature	92.251	98.708	89.220	2.154	93.724
LAStools_city	89.223	99.257	84.012	1.161	91.000
SMRF	89.371	85.568	99.997	28.727	92.221
CSF	85.292	83.327	95.832	32.658	89.143
LAStools_nature with clustering	92.517	99.179	89.201	1.363	93.926
LAStools_city with clustering	89.252	99.340	83.985	1.029	91.019
SMRF with clustering	91.854	88.851	99.985	23.152	94.090
CSF with clustering	88.313	87.902	95.064	24.145	91.343
Proposed method	95.919	97.108	96.392	4.887	96.749

$$\text{Recall} = \frac{TP}{TP + FN} \quad (11)$$

$$\text{Fall-out} = 1 - \frac{TN}{TN + FP} \quad (12)$$

$$F1\text{-score} = 2 * \frac{\text{Precision} * \text{Recall}}{\text{Precision} + \text{Recall}} \quad (13)$$

The proposed method showed overall high indicator values, especially the highest in accuracy and F1 score. As the point cloud contains position information, it is important not only to evaluate accuracy based on the number of points arithmetically but also to conduct a visual inspection. This is because the higher the point density in the data, such as bicycle roads, which have low classification difficulty, the higher the accuracy can be measured regardless of the actual performance of the algorithm.

Fig. 18 shows the result of the visual inspection for each filtering method. The correctly classified data is marked in blue, and the incorrectly classified data is marked in red. Except for the proposed method, there was a common error that classifies points lying far from the levee as a levee point cloud. These errors may lead to arithmetic errors in obtaining attribute information of levee, such as levee elevation.

4.2. Comparison based on levee elevation

Automatic calculation and updating attribute information of levees is key for facility management using digital twins. Accordingly, the levee elevation was automatically calculated from the extracted levee point cloud. The highest Z-value excluding outliers from result levee point

clouds is regarded as the levee elevation in each of the 100 unit point clouds. The calculated levee elevations were compared with the manually measured values and the total station field survey results.

The average error between the manually obtained levee elevation and the value calculated from the result obtained by the proposed method was 0.194 m. The results for the entire dataset are shown in Fig. 19. The results of the automatically estimated levee elevation are displayed according to the number of unit point cloud and are shown in blue. The manually investigated levee elevations are also displayed according to the unit numbers in orange. The point cloud sections were numbered in the upstream direction. The results estimated from the levee point clouds which are extracted from the comparison algorithms are displayed in dotted lines. These graphs show a big differences from the manually investigated values, which means that the levee point cloud extraction results of the comparison algorithms were less accurate.

The average errors between the results calculated from the point cloud results obtained from other comparison methods and the measured value are shown in Table 4. As confirmed in the previous visual inspection, the error of classifying points far from the actual levee location into levee served as a major obstacle in calculating the physical properties of the levee.

A comparison was also conducted with field measurement of the levee elevation by total station. Total station survey was conducted on five survey lines designated as official survey lines by the management authority (MOLIT, 2015). The MAE was 0.130 m, and the root mean square error (RMSE) was 0.161 m, as summarized in Table 5. These results suggest that methods using MLS and digital twin can replace existing methods in river facility management.

4.3. Performance evaluation according to varying parameters

Table 6 shows the performance evaluation result according to varying parameters. The following three key parameters, i.e., segmentation interval, levee slope criteria, and searching radius of DBSCAN were selected and applied to the proposed algorithm to accommodate various scenarios. 16 additional experiments were conducted to provide ranges of input values.

Case 1 represents the same condition applied to the paper. The cases from 2 to 6 indicate that the slope has been changed from 1 to 4, while two other parameters are specified in case 1. The cases from 7 to 11 indicate that the segmentation interval has been changed from 2 m to 50 m, while two other parameters are specified as in case 1. The cases from 12 to 17 indicate that the searching radius of DBSCAN has been changed from 0.05 m to 5 m, while two other parameters are fixed as in case 1.

From cases 2 to 6, MAE significantly increases when the levee slope

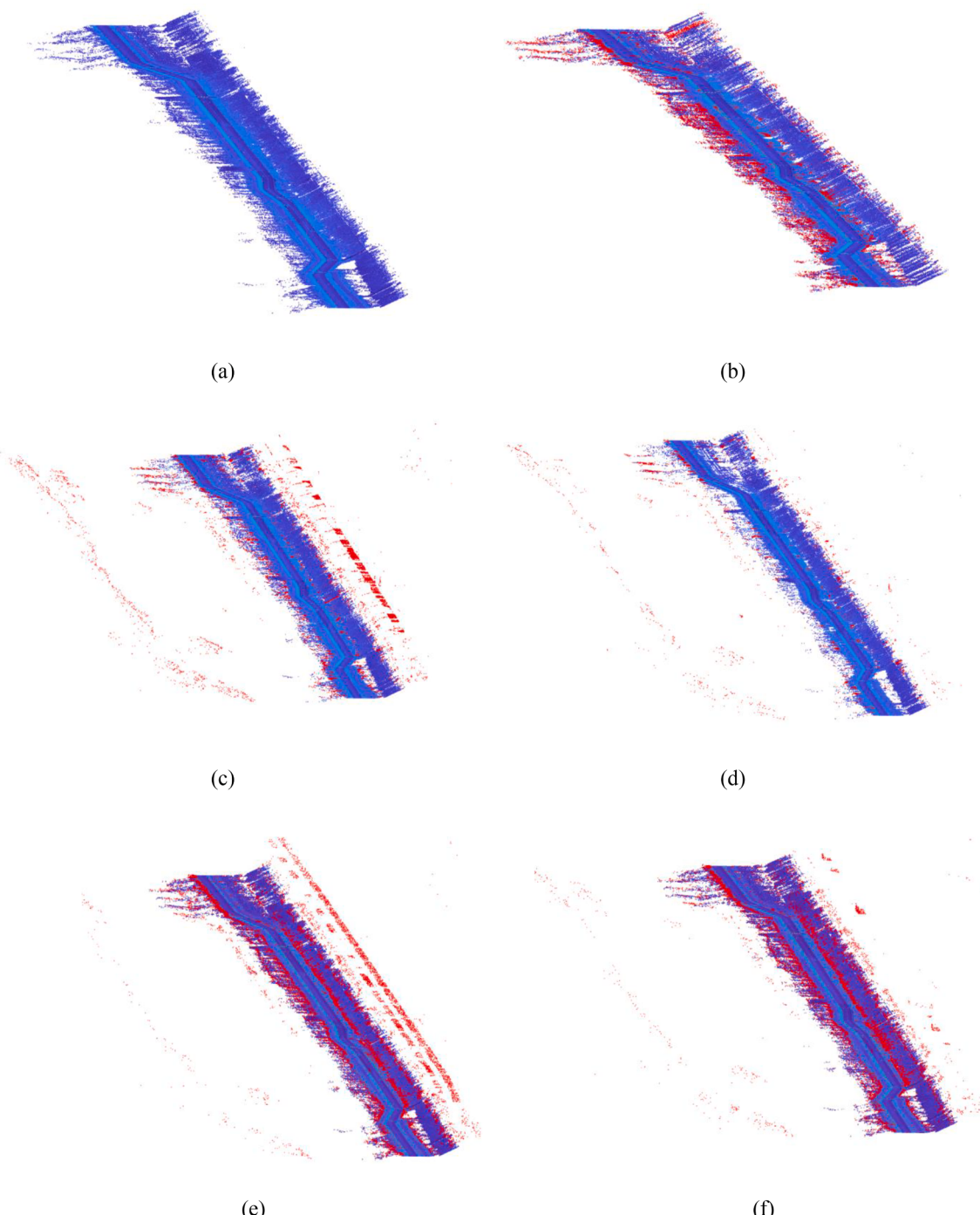


Fig. 18. Comparison of filtering results. The correctly classified data is marked in blue, and the incorrectly classified data is marked in red. (a) manually selected (ground truth); (b) proposed method (c) LAStools_nature; (d) LAStools_city; (e) CSF; (f) SMRF. (For interpretation of the references to color in this figure legend, the reader is referred to the web version of this article.)

deviates from 1:2. The result is due to fact that the levee slope has obvious design criteria. This indicates that the provided slope should be used if there are clear design criteria. From cases 7 to 11, MAE dramatically increases when the segmentation interval is too short. The result seems to happen because the directional equalization step cannot be performed effectively with insufficient levee interval. On the contrary, when the segmentation interval is too long, the accuracy of levee extraction becomes low. From cases 12 to 17, the performance becomes better when the searching radius of DBSCAN is closer to 0.3, which is determined empirically.

5. Conclusions and future work

Digital twins effectively solve problems in the real world through the combination of attribute information and geospatial information. In river facility management, an effective inspection of the levee safety is possible by automatically obtaining the physical properties of the levee through digital twins. Therefore, attempts are being made to build digital twins using vehicle-type MLS in large areas such as rivers. However, studies to extract levee surface from the acquired data are insufficient. This is because the existing ground filtering algorithms can only be applied to data from airborne LiDAR, which does not reflect the

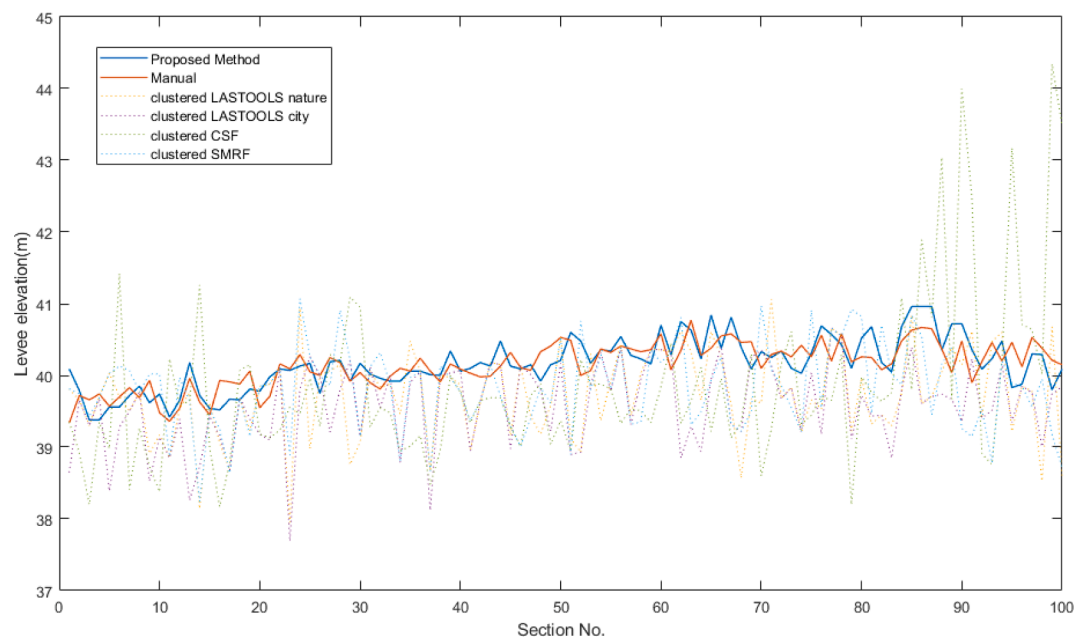


Fig. 19. Levee elevation values obtained with the proposed method (blue), manual measurement (orange) and others (dotted lines). (For interpretation of the references to color in this figure legend, the reader is referred to the web version of this article.)

Table 4

MAEs between levee elevations calculated from each method and manually measured value.

	LASTools_nature	LASTools_city	CSF	SMRF	LASTools_nature with clustering	LASTools_city with clustering	CSF with clustering	SMRF with clustering	Proposed method
MAE (m)	14.684	4.656	14.003	13.108	0.569	0.609	0.878	0.566	0.194

Table 5

Comparison between total station measurement and levee elevation from the algorithm.

Survey line (No.)	Total station measurement (m)	Levee elevation from the algorithm (m)	Absolute Error (m)	MAE (m)	RMSE (m)
12 + 927	39.914	39.790	0.124	0.130	0.161
13 + 166	39.581	39.740	0.159		
13 + 185	39.751	39.650	0.101		
13 + 407	40.068	39.920	0.148		
13 + 656	40.801	40.700	0.101		

characteristics of data acquired through MLS. Therefore, the researchers conducted a study to extract levee surface from data acquired through MLS. To reflect the characteristics of MLS acquired data, directional equalization and density-based clustering with point cloud projection methods were used to extract the levee point cloud, and the levee elevation was estimated from the extracted levee point cloud.

The algorithm was applied to a 1 km study area of Anyang-cheon, and the levee point cloud was extracted and levee elevation values for 100 units according to the GNSS epochs were estimated. Accuracy evaluation was performed using manually made ground truth point clouds. And the levee points clouds extracted by applying existing ground filtering algorithms were utilized for comparison. The performance of the proposed method was also verified with visual inspection and levee elevation assessment which is automatically calculated from the results. As a result of the comparison, the proposed method showed best results in indicators of accuracy and F1 score. This could be verified distinctively in visual inspection. Also the levee elevation could be

Table 6

Performance evaluation according to varying parameters.

No.	Interval (m)	Levee slope	DBSCAN search radius (m)	Accuracy	F1 score	MAE (m)
1	10	1:2	0.3	95.919	96.749	0.194
2	10	1:1	0.3	95.682	96.803	0.767
3	10	1:1.25	0.3	95.332	96.583	0.743
4	10	1:1.5	0.3	95.592	96.744	0.736
5	10	1:3	0.3	94.539	95.825	0.761
6	10	1:4	0.3	93.221	94.742	0.766
7	2	1:2	0.3	91.663	93.552	2.037
8	5	1:2	0.3	90.289	92.384	0.703
9	20	1:2	0.3	90.795	92.777	0.462
10	30	1:2	0.3	88.628	90.934	0.423
11	50	1:2	0.3	84.100	86.821	0.213
12	10	1:2	0.05	93.075	94.654	2.503
13	10	1:2	0.1	94.742	95.999	2.015
14	10	1:2	0.2	95.325	96.416	1.197
15	10	1:2	1	95.292	96.450	0.808
16	10	1:2	3	95.196	96.381	1.546
17	10	1:2	5	94.266	95.710	1.831

extracted most accurately. The mean absolute error compared to the values measured manually from the acquired point cloud was 0.194 m. The mean absolute error compared to the total station measurements was 0.130 m. As a result, it has been shown that the proposed method can be a good option in building the digital twin of the levee. The benefits of levee management using MLS and the automatic levee elevation estimation algorithm presented in this study compared to the existing levee management methods can be summarized as follows:

First, MLS-based management is rapid and repeatable. It took only 5

min to acquire data for the 1 km study alignment. Thus, the proposed method is efficient compared to the existing method using a total station, which takes several days. Second, more detailed levee management is possible. Using MLS and the algorithm, 1 km of the study area was segmented into 100 units, and each unit's levee elevation values were estimated. Compared to the existing methods, which can only inspect the same levee area on five survey lines, more detailed management is possible with the MLS method. Third, the MLS enables comprehensive levee inspections. Because the MLS obtains object shape, color, and location information, the infrastructure manager can get more comprehensive information beyond the numeric data.

There are some points to take into consideration to get the best results using the proposed algorithm.

First, accurate construction design criteria for levee are necessary because the algorithm improves the accuracy by imposing the numerical design value as a constraint. As the levee is an engineering structure built on a legitimate design, the algorithm users are recommended to identify and utilize the design information in advance. In this study, the design levee elevation value is used to evaluate the accuracy of the clustering results and to determine whether additional clustering is necessary. Also, the design levee slope value is adopted as the ratio between grid size and Z-threshold while extracting the lowest points. Data loss will be significant when the grid size is too large compared to the Z-threshold. And vice versa, the final surface turns out to be too thick, or the computational load will be too heavy.

Second, it is necessary to figure out the characteristics of the target area and the specification of the individual MLS utilized. In this study, point cloud data was segmented based on the GNSS epoch. However, if the target area has severe curvature while the GNSS epoch is relatively large, the effect of the severe curvature will remain and cause a bad outcome throughout the remaining procedure of the algorithm. In this case, an error may occur while applying directional equalization and projective clustering. Therefore, the segmentation interval needs to be adjusted to circumvent the effect of the curvature.

Third, the algorithm assumes that the LiDAR data includes the bare ground of the levee surface. In the case of using MLS, the laser signal emitted from MLS arrives on the bare ground of the levee, avoiding obstacles such as grass and shrubs to obtain the information. In this case, the lowest points of the acquired data can be considered to represent the levee surface. However, if the target levee is covered with obstacles too densely so that there never exists any space for the laser signal's arrival, the bare ground point cloud would not be included in the data. In such a case, an extracted point cloud may not represent the levee surface.

Based on the experiment result and despite of some limitations, the extracted levee surface would be used as a basic data for levee management. Furthermore, the researchers are developing levee management algorithms to obtain more information from extracted levee point clouds, such as estimation of the levee slope, detection of changes, and automatic building information model (BIM) construction. In addition, other forms of MLS, such as MLS operated in a backpack instead of a vehicle that collects data while walking, would be helpful for levee management, and related research being performed.

Data availability statement.

Some or all data, models, or code generated or used during the study are proprietary or confidential in nature and may only be provided with restrictions.

CRediT authorship contribution statement

Jisang Lee: Conceptualization, Methodology, Software, Writing – original draft. **Suhong Yoo:** Software. **Cheolhwan Kim:** Data curation. **Hong-Gyoo Sohn:** Writing – review & editing, Investigation.

Declaration of Competing Interest

The authors declare that they have no known competing financial

interests or personal relationships that could have appeared to influence the work reported in this paper.

Data availability

The data that has been used is confidential.

Acknowledgements

This research was supported by a grant (20009742) of Ministry-Cooperation R&D program of Disaster-Safety, funded by Ministry of the Interior and Safety (MOIS, Korea). And this work was supported by Korea Environment Industry & Technology Institute (KEITI) through Advanced Water Management Research Program, funded by Korea Ministry of Environment (MOE) (21AWMP-B121100-06). Also, we would like to thank Editage (www.editage.co.kr) for English language editing.

References

- Akiyama, N., Nishiyama, S., Sakita, K., Song, J., Yamazaki, F., 2021. River Levees Monitoring Using Three Dimensional Laser Point Clouds with SLAM Technology. *Sustain. Civ. Infrastructures* 14–22.
- Axelsson, P., 2000. DEM generation from laser scanner data using adaptive TIN models. *Int. Arch. Photogramm. Remote Sens.* 33, 110–117.
- Błaszczyk-Bąk, W., Janowski, A., Kamiński, W., Rapiński, J., 2015. Application of the Msplit method for filtering airborne laser scanning data-sets to estimate digital terrain models. *Int. J. Remote Sens.* 36, 2421–2437.
- Cai, S., Zhang, W., Qi, J., Wan, P., Shao, J., Shen, A., 2018. Applicability analysis of cloth simulation filtering algorithm for mobile LiDAR point cloud. In: International Archives of the Photogrammetry, Remote Sensing and Spatial Information Sciences - ISPRS Archives. pp. 107–111.
- Casas, A., Riaño, D., Greenberg, J., Ustin, S., 2012. Assessing levee stability with geometric parameters derived from airborne LiDAR. *Remote Sens. Environ.* 117, 281–288.
- Che, E., Jung, J., Olsen, M.J., 2019. Object recognition, segmentation, and classification of mobile laser scanning point clouds: A state of the art review. *Sensors (Switzerland)* 19.
- Che, E., Olsen, M.J., 2017. Fast ground filtering for TLS data via Scanline Density Analysis. *ISPRS J. Photogramm. Remote Sens.* 129, 226–240.
- Chen, C., Li, Y., Yan, C., Dai, H., Guolin, L., Guo, J., 2016. An improved multi-resolution hierarchical classification method based on robust segmentation for filtering ALS point clouds. *Int. J. re* 37, 950–968.
- Chen, Q., Gong, P., Baldocchi, D., Xie, G., 2007. Filtering airborne laser scanning data with morphological methods. *Photogramm. Eng. Remote Sens.* 2, 175–185.
- Chen, Z., Gao, B., Devereux, B., 2017. State-of-the-art: DTM generation using airborne LiDAR data. *Sensors* 17 (1), 150.
- Chen, S., Zhang, Z., Zhong, R., Zhang, L., Ma, H., Liu, L., 2021. A dense feature pyramid network-based deep learning model for road marking instance segmentation using MLS point clouds. *IEEE Trans. Geosci. Remote Sens.* 59, 784–800.
- Choi, Y., Farkoushi, M.G., Hong, S., Sohn, H.G., 2019. Feature-based matching algorithms for registration between LiDAR point cloud intensity data acquired from MMS and image data from UAV. *J. Korean Soc. Surv. Geod. Photogramm. Cartogr.* 37, 453–464.
- Choung, Y., 2014. Mapping levees using LiDAR data and multispectral orthoimages in the Nakdong River Basins, South Korea. *Remote Sens.* 6, 8696–8717.
- Ester, M., Kriegel, H.-P., Sander, J., Xu, X., 1996. A Density-Based Algorithm for Discovering Clusters in Large Spatial Databases with Noise. In: KDD-96. pp. 635–654.
- Evans, J.S., Adrew, H.T., 2007. A multiscale curvature algorithm for classifying discrete return LiDAR in forested environments. *IEEE Trans. Geosci. Remote Sens.* 45, 1029–1038.
- Gézero, L., Antunes, C., 2017. An efficient method to create digital terrain models from point clouds collected by mobile lidar systems. In: International Archives of the Photogrammetry, Remote Sensing and Spatial Information Sciences. pp. 289–296.
- Hong, S., Park, I., Lee, J., Lim, K., Choi, Y., Sohn, H., 2017. Utilization of a Terrestrial Laser Scanner for the Calibration of Mobile Mapping Systems. *Sensors* 17 (3), 474.
- Husain, A., Vaishya, R.C., 2016. A time efficient algorithm for ground point filtering from mobile LiDAR data. In: In: 2016 International Conference on Control, Computing, Communication and Materials (ICCCCM). Institute of Electrical and Electronics Engineers Inc., pp. 1–5.
- Ibrahim, S., Lichti, D., 2012. Curb-Based Street Floor Extraction From Mobile Terrestrial Lidar Point Cloud. In: The International Archives of the Photogrammetry, Remote Sensing and Spatial Information Sciences. pp. 193–198.
- Jiang, F., Ma, L., Broyd, T., Chen, K., 2021. Digital twin and its implementations in the civil engineering sector. *Autom. Constr.* 130, 103838.
- Jung, J., Che, E., Olsen, M.J., Parrish, C., 2019. Efficient and robust lane marking extraction from mobile lidar point clouds. *ISPRS J. Photogramm. Remote Sens.* 147, 1–18.

- Kobler, A., Pfeifer, N., Ogrinc, P., Todorovski, L., Oštr, K., Džeroski, S., 2007. Repetitive interpolation: A robust algorithm for DTM generation from Aerial Laser Scanner Data in forested terrain. *Remote Sens. Environ.* 108, 9–23.
- Kraus, K., Pfeifer, N., 1998. Determination of terrain models in wooded areas with airborne laser scanner data. *ISPRS J. Photogramm. Remote Sens.* 53, 193–203.
- Kriegel, H.-P., Kröger, P., Sander, J., Zimek, A., 2011. Density-based clustering. Wiley Interdiscip. Rev. Data Min. Knowl. Discov. 1, 231–240.
- Lee, J., Kwon, J.H., Keum, Y.M., Moon, J., 2011. The Update of Korean Geoid Model based on Newly Obtained Gravity Data. *J. Korean Soc. Surv. Geod. Photogramm. Cartogr.* 29, 81–89.
- Lee, J., Hong, S., Park, I., suk Mohammad, G.F., Kim, C., Sohn, H.-G., 2021. Levee Maintenance Using Point Cloud Data Obtained from a Mobile Mapping System. *KSCE J. Civ. Environ. Eng. Res.* 41, 469–475.
- Li, Y., Yong, B., Wu, H., An, R., Xu, H., Xu, J., He, Q., 2014. Filtering airborne lidar data by modified white top-hat transform with directional edge constraints. *Photogramm. Eng. Remote Sens.* 9, 133–141.
- Lin, X., Zhang, J., 2015. Segmentation-based ground points detection from mobile laser scanning point cloud. In: The International Archives of the Photogrammetry, Remote Sensing and Spatial Information Sciences. p. 99.
- Liu, X., 2008. Airborne LiDAR for DEM generation: some critical issues. *Prog. Phys. Geogr. Earth Environ.* 32, 31–49.
- Meng, X., Currit, N., Zhao, K., 2010. Ground filtering algorithms for airborne LiDAR data: A review of critical issues. *Remote Sens.* 2, 833–860.
- Meng, X., Wang, L., Silván-Cárdenas, J.L., Currit, N., 2009. A multi-directional ground filtering algorithm for airborne LiDAR. *ISPRS J. Photogramm. Remote Sens.* 64, 117–124.
- MOLIT, 2015. Report for river basic plan of Anyang-cheon. Anyang.
- MOLIT, 2018. Korean Design Standard 51 50 05:2018 levee. Republic of Korea.
- Mongus, D., Lukac, N., Zalik, B., 2014. Ground and building extraction from LiDAR data based on differential morphological profiles and locally fitted surfaces. *ISPRS J. Photogramm. Remote Sens.* 93, 145–156.
- Olsen, M.J., 2013. Guidelines for the Use of Mobile LiDAR in Transportation Applications.
- Pirotti, F., Guarneri, A., Vettore, A., 2013. Ground filtering and vegetation mapping using multi-return terrestrial laser scanning. *ISPRS Int. J. Geo-Information* 76, 56–63.
- Rapinski, J., Kaminski, W., Janowski, A., Blaszcak-Bak, W., 2011. ALS Data Filtration with Fuzzy Logic. *J. Indian Soc. Remote Sens.* 39, 591–597.
- Rasheed, A., San, O., Kvamsdal, T., 2020. Digital twin: Values, challenges and enablers from a modeling perspective. *IEEE Access* 8, 21980–22012.
- Rodríguez-Caballero, E., Afana, A., Chamizo, S., Solé-Benet, A., Cantón, Y., 2016. A new adaptive method to filter terrestrial laser scanner point clouds using morphological filters and spectral information to conserve surface micro-topography. *ISPRS J. Photogramm. Remote Sens.* 117, 141–148.
- Saye, S.E., van der Wal, D., Pye, K., Blott, S.J., 2005. Beach-dune morphological relationships and erosion/accretion: An investigation at five sites in England and Wales using LiDAR data, 72, 128–155.
- Serna, A., Marcotegui, B., 2013. Urban accessibility diagnosis from mobile laser scanning data. *ISPRS J. Photogramm. Remote Sens.* 84, 23–32.
- Serna, A., Marcotegui, B., 2014. Detection, segmentation and classification of 3D urban objects using mathematical morphology and supervised learning. *ISPRS Int. J. Geo-Information* 93, 243–255.
- Shanbari, H.A., Blinn, N.N., Issa, R.R., 2016. Laser scanning technology and BIM in construction management education. *J. Inf. Technol. Constr.* 21, 204–217.
- Sithole, G., Vosselman, G., 2004. Experimental comparison of filter algorithms for bare-Earth extraction from airborne laser scanning point clouds. *ISPRS J. Photogramm. Remote Sens.* 59, 85–101.
- Teo, T.A., Yu, H.L., 2015. Empirical radiometric normalization of road points from terrestrial mobile lidar system. *Remote Sens.* 7, 6336–6357.
- Tyagur, N., Hollaus, M., 2016. Digital terrain models from mobile laser scanning data in Moravian Karst. In: International Archives of the Photogrammetry, Remote Sensing and Spatial Information Sciences - ISPRS Archives. pp. 387–394.
- Vallet, B., Papelard, J.P., 2015. Road orthophoto/dtm generation from mobile laser scanning. In: ISPRS Annals of the Photogrammetry, Remote Sensing and Spatial Information Sciences. pp. 377–384.
- Vosselman, G., 2000. Slope based filtering of laser altimetry data. In: International Archives of Photogrammetry and Remote Sensing. pp. 935–942.
- Wang, C., Menenti, M., Stoll, M.-P., Feola, A., Bellucci, E., Marani, M., 2009. Separation of ground and low vegetation signatures in LiDAR measurements of salt-marsh environments. *IEEE Trans. Geosci. Remote Sens.* 47, 2014–2023.
- Wu, B., Yu, B., Huang, C., Wu, Q., Wu, J., 2016. Automated extraction of ground surface along urban roads from mobile laser scanning point clouds. *Remote Sens. Lett.* 7, 170–179.
- Yadav, M., Singh, A., Remote, B.L.-I.J. of, 2017, undefined, 2017. Extraction of road surface from mobile LiDAR data of complex road environment. Taylor Fr. 38, 4655–4682.
- Yang, B., Wei, Z., Li, Q., Li, J., 2012. Automated extraction of street-scene objects from mobile lidar point clouds. *Int. J. Remote Sens.* 33, 5839–5861.
- Yu, Y., Li, J., Guan, H., Wang, C., 2015. Automated Extraction of Urban Road Facilities Using Mobile Laser Scanning Data. *IEEE Trans. Intell. Transp. Syst.* 16, 2167–2181.
- Zhang, W., Qi, J., Wan, P., Wang, H., Xie, D., Wang, X., Yan, G., 2016. An easy-to-use airborne LiDAR data filtering method based on cloth simulation. *Remote Sens.* 8, 501.